International Journal of Innovative Computing, Information and Control
Volume **19**, Number **2**, April **2023**

ICIC International ©2023 ISSN 1349-4198
pp. 365–383

AUTOMATED DETECTION OF VISUAL FLAWS AND THEIR LOCATING SIDES ON FLAT TRANSPARENT WORKPIECES WITH TEXTURED BACKGROUND

Hong-Dar Lin[1,*], Zi-Ting Qiu[1] and Chou-Hsien Lin[2]

[1]Department of Industrial Engineering and Management
Chaoyang University of Technology
No. 168, Jifong East Road, Wufong District, Taichung 41349, Taiwan
ziting_chiu@aseglobal.com
*Corresponding author: hdlin@cyut.edu.tw

[2]Department of Civil, Architectural, and Environmental Engineering
The University of Texas at Austin
301, East Dean Keeton Street, Austin, Texas 78712-0273, USA
chslin@utexas.edu

Received August 2022; revised November 2022

Abstract. *Transparent materials are widely used in many consumer products today, often in the form of flat sheets. The flatness and transparency of these workpieces complicate the quality control process, as defects on either side of a workpiece are simultaneously visible, and determining the exact side on which the defect occurred is difficult. This study proposes an optical inspection system that combines flaw detection and determination of the location of the flaw in the fabrication of flat transparent workpieces. We first apply the time-frequency analysis based on the Hilbert-Huang transform to enhancing the contrast between the flaws and the background. Second, statistical interval estimation is used to segment the background and flaws to achieve flaw detection. Third, the detected flaws on both sides of the substrates are combined and numbered for feature extraction. Fourth, a random forest based on ensemble learning is applied to judging where the flaws occur and whether they are on the front or back of the transparent substrates. The experimental results achieved a flaw detection rate of 86.67% in all real defects, with a false alarm rate of 2.32% in the detected defects. The correct location determination rate for the flaw is 98.62% on the front and back sides of the touch panels.*

Keywords: Transparent workpieces, Textured background, Optical inspection, Flaw detection, Incident location determination, Time-frequency analysis, Ensemble learning

1. **Introduction.** Transparent materials have visual penetration properties that are useful in many products, such as glass, transparent substrates, polarizing films, diffusers, and optical fibers. When these transparent workpieces are photographed by imaging equipment for quality control purposes, afterimages and noise often appear in the captured images due to the material's astigmatic properties and differences in background illumination. Moreover, since the workpieces are transparent, defects on both sides (front and back) of the workpiece are simultaneously visible in the same image and the exact location of the defect is difficult to determine. To ensure the quality of transparent products, it is vital to develop a more specialized visual inspection system for transparent workpieces.

Touch panels commonly used in electronic devices today are composed of a multilayer film and two or more transparent substrate glass. The surface of a touch panel is transparent glass with conductive wires inside to achieve the purpose of touch control. The panel

DOI: 10.24507/ijicic.19.02.365

has regular conductive electrodes and conductive wires as a background. According to the design and functional considerations of different manufacturers, there are many textured background patterns of transparent workpieces with various conductive electrodes and conductive lines. The capacitive touch panel has the advantages of waterproofness, dust proofness, oil resistance, fast response, etc., and is favored by the market. The panel has a transparent glass surface and a regular texture of an inner transparent conductive film.

Common flaws that affect transparent workpieces include scratches, cracks, dirt intrusion, watermarks, etc. These flaws are mainly caused by improper cleaning or neglect during handling. Surface flaws of transparent workpieces can be classified into two main types based on their shape: linear flaws that are directional, for instance, scratches and cracks; and area flaws that are irregular in shape and low contrast, including dust intrusion and watermarks. The existence of flaws not only affects the appearance and quality of the product but may also seriously impact product functionality. Correctly identifying the side on which the flaws occurred is therefore vital for quality control and can provide insight into the causes of these defects.

Usually, two focused images are required to distinguish front and back flaws, with one image taken from each side of the panel and analyzed. Figure 1 shows a testing sample including a linear flaw and an area flaw. Two images of the sample are captured while (a) the focus is on the front side and (b) the focus is on the back side, respectively. The red ovals in the figures represent the flaws that occur on the front sides, and the blue squares represent those on the back sides. As shown in Figure 1, the same flaws appear in the images focused on the front and back sides, and the visual difference between the two is insignificant.

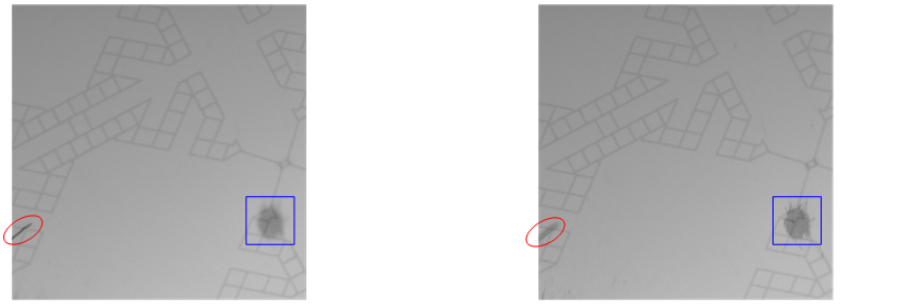

(a) Flaw image acquired with a front focus setting (b) Flaw image acquired with a back focus setting

FIGURE 1. Testing images containing a linear flaw and an area flaw acquired with various focus settings

Surface flaw detection on flat transparent workpieces with textured backgrounds needs to overcome the following challenges: First, due to astigmatism and light transmittance of transparent materials, captured images of the workpiece are prone to noise and afterimages; Second, the variety of background textures on the transparent workpieces can interfere with flaw detection; Third, for relatively thin workpieces, the difference between the front and back images is small, so determining the location of flaws becomes more challenging; Fourth, the same flaw will appear in both the front and back images, making it difficult to determine the actual location of the flaw.

Because the touch panel is a high-precision, thin-thickness optoelectronic product, the flaws are tiny flaws that may repeatedly appear on the front and back sides of panels, which may easily cause misjudgment of identification. In the production process of the product, the processing requirements and flaw handling standards of the front and back are different. Distinguishing the location of flaws on the front and back can reduce misjudgment and improve the efficiency and benefit of process improvement. Therefore, we

propose a vision system based on machine learning technology to perform flaw detection and determination of incident location, that is, the flaw occurs on the front or back of the transparent workpiece.

The rest of the article is composed as follows. First, we review the articles on current techniques of visual inspection systems for transparent products. Second, we describe the proposed image procedures to detect flaws and determine the side of occurrence of the transparent workpieces. Third, we conduct tests and assess the performance of the suggested models using traditional techniques. Finally, we conclude the contributions and indicate further directions.

2. **Literature Review.** Transparency in materials allows light to travel through them unaffected, thus making the materials see-through. Transparent substrates are widely used as base materials for the manufacture of optical and electronic products, such as display optical films, lighting optics, thin packaging films, display panels, touch panels, and electronic components. Xu et al. [1] developed a geometry and optical inspection system to create fringe patterns in automotive glass for flaw detection. Lin et al. [2] proposed a Hough transform-based voting scheme to inspect distortion flaws in curved windscreen glass of vehicles. Currently, many works of literature discuss the detection and classification of surface flaws in transparent workpieces [3]. This type of transparent material has a uniform or random texture in the background, and the flaws are more obvious. Few studies discuss the detection of flaws in transparent workpieces with structural texture backgrounds. Test samples with textured backgrounds are more difficult to inspect visually.

Repeating patterns are everywhere, especially in man-made objects. They provide structural and geometric or semantic clues about the elemental structures of which repeated patterns are composed. The detection of repeated patterns can benefit many algorithms in computer vision and graphics [4,5]. Conductive glass is transparent glass with repeated patterns (structural lines). It has the function of conducting electricity through the conductive film. It has been widely used in optical devices. Lin and Tsai [6] used the spectral characteristics of the Fourier transform and matched them with cross-shaped filtering to eliminate parts with higher energy values to attenuate the background texture. Hung and Hsieh [7] used the characteristics of the periodic pattern of the sensing texture to adaptively learn each background pattern and then compare it with the standard board to extract flaws to achieve the effect of flaw detection. The problem of detecting flaws is complicated by the difference in the type of flaw and the textured background of the touch panel image [8]. Chiu and Lin [9] proposed a wavelet transform-based method to check the flaws in the appearance of touch panels with a variation in the structural texture of the background. Jian et al. [10] proposed a positioning based on image contours for the glass of the mobile phone screen that can identify screen flaws. In reviewing the literature above, they all detect and classify the surface flaws of touch panels [6,9,11-13], but few studies discuss the issue of the transparent panel flaws that occur on the front side or the back side of the panel.

When the front and back of the product are similar in appearance or are made of transparent materials, there will be a problem that the front and back sides are difficult to distinguish, resulting in many difficulties in identification, measurement, and detection. Carlson and Le [14] proposed that wafers should be inspected on both front and back sides. When there is a flaw on the back side, the front side at the same position will be compared and correlated. Minami et al. [15] proposed that the source of transparent substrate flaws is the attachment of contaminants to the patterned front side and fewer flaws occur on the back side. Gevigney [16] proposed a method using Doppler laser velocimetry to inspect the front and back sides of transparent wafers. Furthermore, different levels of processing

and quality requirements will be applied to the front and back of the product during the manufacturing process, so it is necessary to evaluate the front and back of the product to ensure its quality of the product [17].

The glass substrate of the touch panel is transparent and contains a variety of structural lines. The flaws generated in the process are even more diverse. Many scholars have discussed this aspect, mainly to remove certain lines or only to detect some specific flaws [6,9]. For the detection of some specific textures, the position of the sample must be fixed to keep the same orientation of the texture in the image, and then remove the background. This method has limited efficiency and benefit for workpieces with various texture backgrounds. At present, few methods can deal with multiple types of textures and flaws at the same time. The time-frequency analysis based on the Hilbert-Huang transform (HHT) proposed in this study is different from the above research methods. It uses the decomposition of a bidimensional empirical mode decomposition (BEMD) image to attenuate the background and increase the contrast between the flaws and the background. The method consists of empirical mode decomposition (EMD) and Hilbert transform (HT) [18,19]. Guo et al. [20] applied the time-frequency energy matrix of a distribution network to the sampled fault signal using the HHT method. The EMD is converted from one-dimensional to BEMD, which is often used in flaw detection of agricultural fruits [21], suppression of image noise [22], face recognition, and texture analysis. HHT has a good effect in many different fields, such as image processing, fault detection, and industrial inspection [21,23].

The decision tree is an attractive classifier due to its fast execution speed. However, for problems with high complexity, the precision of data analysis is not high. Kwon et al. [24] applied random forests to fast defect detection for various types of surface defects in wood without changing model parameters. Therefore, a random forest is a combination of tree predictors, each based on a random and independent distribution of all trees in the forest using the same method [25]. Kamalalochana et al. [26] developed an optical inspection system to inspect apple leaves and use random forests as classifiers to detect diseases in apple leaves. Shipway et al. [27] aimed to perform a fluorescent penetrant inspection to detect and classify surface flaws using a random forest model in the aerospace industry. Dong et al. [28] developed a random forest-based automatic inspection system for aerospace welds in X-ray images to locate the weld and examine it for defects. Jr. Piedad et al. [29] used machine learning to classify bananas for classification and the results show that the random forest has good classification results and accuracy in both training and testing. The random forest method has many different application fields, such as food grading, and insect and plant classification, and has a good effect [30,31].

The purpose of this research is to develop an automatic flaw detection and flaw location determination system for transparent workpieces with textured backgrounds, using the framework of machine vision. Therefore, this study first discusses the inspection items of high-precision processing of transparent glass that are highly based on personnel experience and knowledge of the properties of the material. We propose a novel system development for flaw detection and side determination of flaw locations. Through the developed optical inspection system, the production of transparent workpieces can achieve a higher overall quality.

3. **Proposed Method.**

This research aims to identify the flaws on the surfaces of the transparent workpiece with regular background lines and to judge the incident location of the flaw in the transparent workpiece. The proposed approach is divided into five steps. First, to compare the imaging difference of the same flaw in two images, two testing images are taken when the workpiece is individually captured with a focus on the front

side and a focus on the back side. Second, by applying the HHT method to attenuating the background texture and then enhancing the flaw contrast, we use the BEMD scheme to achieve the effect of attenuating the background texture and the HT to achieve the effect of flaw enhancement. Third, a statistical interval estimation method is applied to the enhanced image for separating flaws from the background, and then we merge the detected flaws into one image. Fourth, we perform the flaw numbering according to the flaw position on the merged image, and then extract the feature vector of each numbered flaw for further classification. Fifth, the random forest method is applied to judging the flaw incident location of the transparent workpiece by classifying the numbered flaws into front flaws, back flaws, and non-flaws.

The HHT is specifically designed to handle data from nonstationary and nonlinear processes without any assumptions or assumed basis functions [18]. The main characteristics of the HHT are its adaptive signal decomposition and filtering in the temporal/spatial domains [19]. Therefore, the proposed HHT-based method can reduce the influence of different texture angles caused by different workpiece placements, and the influence of different background textures on this method is lower, and more types of flaws can be detected.

3.1. **Image capture.** Testing samples with a thickness of 1.67 mm, a width of 132 mm, and a length of 220 mm are randomly selected from the fabrication line of a touch panel manufacturer. To distinguish whether the flaw is located on the front or the back side, it is necessary to take two images with a focus on the front side and a focus on the back side, respectively. By capturing a local area of a panel, the imaging differences between a front focus and a back focus are displayed in the gray level variations and sharpness of the flaw. The local detailed information will help judge whether the flaw occurs on the front or the back side. Because the touch panel has texture, it needs to be illuminated with a blue coaxial light source. The touch panel is placed on the inspection platform and the high-magnification lens is used to take images of a local area so that texture and flaws can be presented in the captured images. Figure 2 illustrates the setup of the image capture devices and the arrangement of the image acquisition apparatus to capture a testing touch panel. To acquire the digital imaging of a testing panel with proper intensity, the lighting control of the environment is also important when acquiring images.

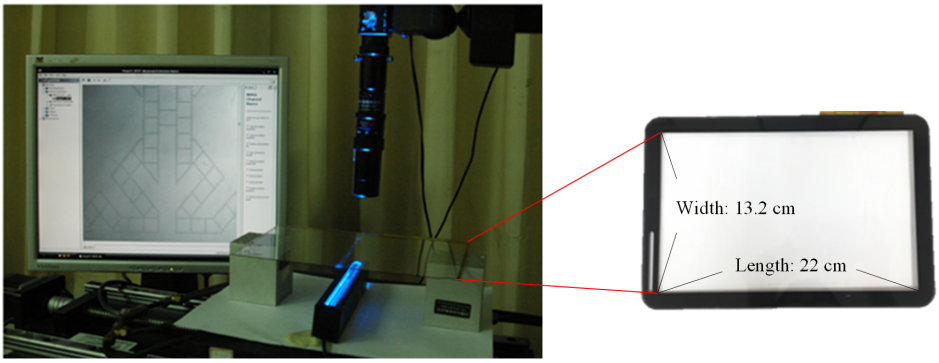

FIGURE 2. Schematic diagram of the setup of the experimental hardware for image acquisition

3.2. **Flaw enhancement and detection.** Since the background conductive lines of the transparent workpiece will interfere with the detection of surface flaws, it is necessary to reduce the influence of the background texture and highlight the contrast of the flaws to facilitate subsequent flaw detection. In the flaw enhancement stage, this study applies the

HHT method to the captured front and back images, respectively. The HHT method is applied to attenuating the background texture and then enhancing the contrast of flaws. We use the BEMD scheme to decompose a testing image into a frequency image and a residual image and then perform the HT conversion on the two decomposed images, respectively, to achieve the effect of attenuating the background texture. After that, we extract the real part of the normalized HHT image, which can further increase the contrast between the flaw and the background to achieve the effect of flaw enhancement.

For image processing and analysis, BEMD is required to extract two-dimensional intrinsic mode function (IMF) frequency images. After the transparent workpiece image in this study is decomposed by BEMD, it is decomposed from high frequency to low frequency based on the image frequency, and a testing image $g(m,n)$ is decomposed into two images, which are an IMF frequency image $IMF_1(m,n)$ and a residual image $r_j(m,n)$ respectively, as follows,

$$g(m,n) = \sum_{i=1}^{j} IMF_i(m,n) + r_j(m,n), \tag{1}$$

where $IMF_i(m,n)$ is the i frequency image generated after the BEMD decomposition.

In the frequency images decomposed by BEMD, the first frequency image contains most of the local features in the original data, whereas the residual image contains fewer local features. The method uses the calculation of local maxima and minima to decompose the image through the average envelope of the cubic curve into a frequency image and a residual image. The first frequency image represents the high frequency in the image. The clearer the background texture of the transparent workpiece and the texture characteristics of the flaws, the more detailed the edge of the image will be, and these details will be preserved in this frequency image. The residual image is a low-frequency image, and the outline of the image begins to appear blurred. Only the outline of the image can be seen, but the details cannot be seen. Figure 3 shows the decomposition results of the front and back flaw images.

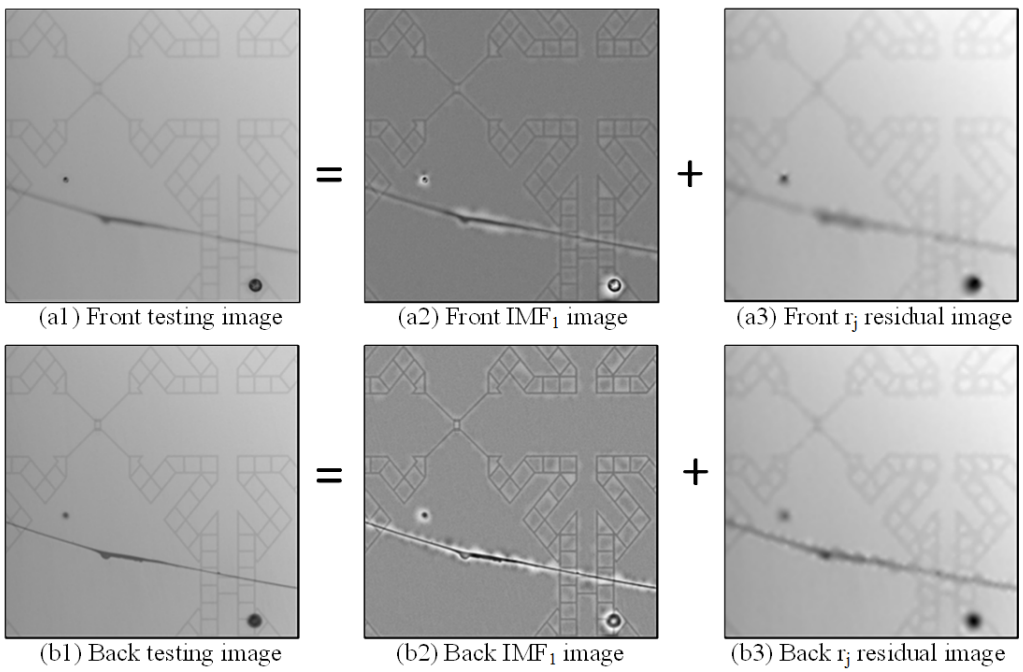

FIGURE 3. Decomposition results of the front and back flaw images by BEMD scheme

Since the BEMD needs to generate the envelope through multiple iterative screening processes, each image needs to be decomposed through a large number of operations. The more images are decomposed, the more process iterations are used. The stopping criterion set in standard deviation (SD) will affect the process iteration of an image. The more process iterations, the longer the execution time, maybe resulting in a waste of execution time. Therefore, the number of decomposed images (i) and the stopping criterion (T) are the most important parameters in the BEMD.

The Hilbert transform is performed on the decomposed image, which is convolved $1/\pi$ through the impulse response, it conducts the extraction of the real instantaneous signal of the image. In this study, HT conversion is performed on the IMF_1 frequency image and the residual image r_j respectively, we will obtain the complex frequency image of IMF_1 and r_j. The complex frequency images $HX_i(s,t)$ and $HX_{r_j}(s,t)$ of the IMF_1 and r_j are expressed as

$$HX_i(s,t) = IMF_i(m,n) \times \frac{1}{\pi} = R_i(s,t) + I_i(s,t) \tag{2}$$

$$HX_{r_j}(s,t) = r_j(m,n) \times \frac{1}{\pi} = R_j(s,t) + I_j(s,t) \tag{3}$$

After HT transformation, the flaws in the IMF_1 frequency image are highlighted and the background of the frequency image becomes smoother. The two images are accumulated to become an accumulated image after performing HHT. The background texture in this cumulative HHT image is attenuated, but the contrast between the flaws and the background is low. Since the grayscale value of the accumulated image is between $[0, 1]$, this study uses the normalization method to convert the grayscale value to $[0, 255]$, so that the difference between the light and dark contrast of the image is widened. By increasing the contrast of the grayscale values through normalization, the image can be presented more clearly.

After the BEMD decomposition and HT conversion process, the HHT conversion is completed. In this study, the IMF frequency flaw images are selected after HHT conversion for enhancement, and the background is diluted. This method of enhancing flaws does not require fixed workpiece orientation and capture position, nor does it need to know the characteristics of the background texture in advance to remove the background. This method is beneficial to remove backgrounds with complex regular textures and is suitable for various texture backgrounds, avoiding the disadvantage that the flaws that overlap with the background will be removed together when the background is removed. When the HHT method performs BEMD decomposition, it needs to iteratively perform the interpolation calculation and the envelope process on the image, and it takes a long time to complete the decomposition process.

After the test image undergoes HHT conversion, the image pixels become complex data types, as shown in Equation (4). There are real and imaginary numbers in the values. The real part has more information containing analytical signals with more texture features, while the imaginary part has less information, so the imaginary numbers can be discarded without losing the major information. Comparisons of the real parts and the imaginary parts of the front and back normalized HHT images are shown in Figure 4. The extracted imaginary image is rendered black and the information in the image cannot be preserved. We further normalize the accumulated HHT image and extract the real number part with information to increase the contrast between the flaw and the background, that is, extract the real number part of the image in Equation (4) as Equation (5).

$$nor(s,t) = R(s,t) + I(s,t) \tag{4}$$

$$real(m,n) = R(s,t) \tag{5}$$

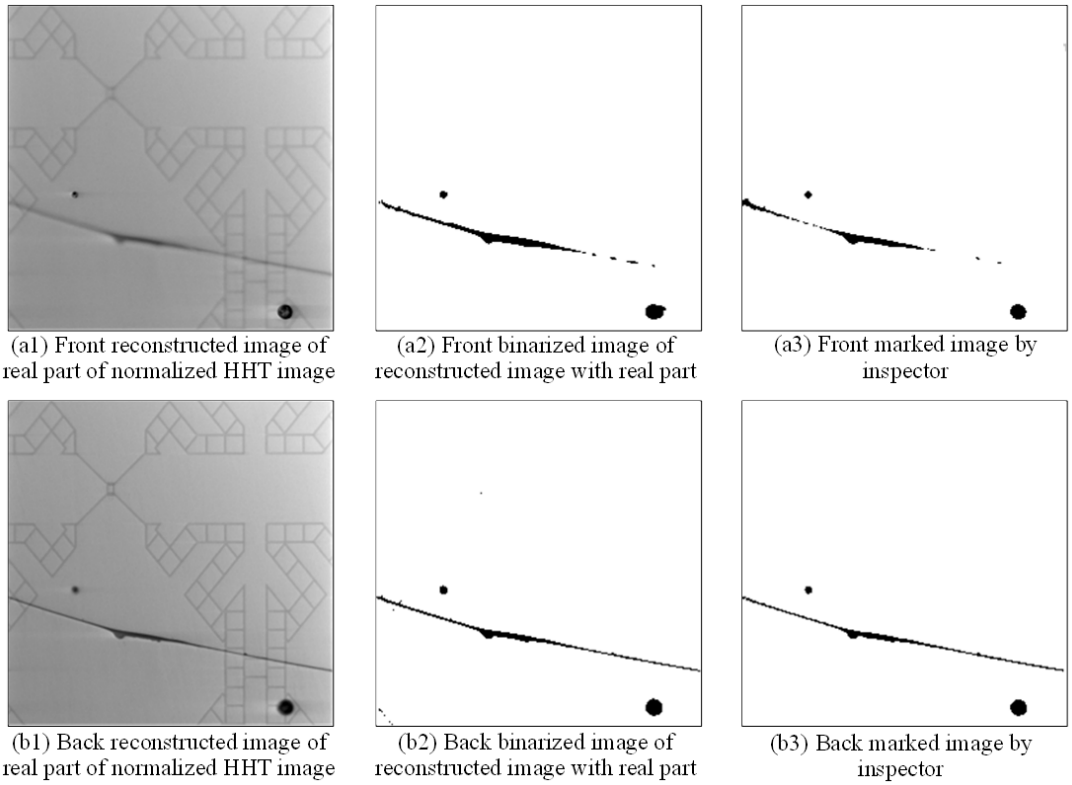

FIGURE 4. The reconstructed and binarized images of the real parts of the front and back normalized HHT images

When a testing image undergoes HHT conversion to achieve the effect of background texture attenuation and flaw enhancement, the textured background and flaws have high contrast at this time. The statistical interval estimation method is used to select the appropriate threshold in image segmentation to separate flaws and backgrounds. If the value is set to less than the threshold, the flaw is displayed in black, and if the value is greater than the threshold, the background is displayed in white. After dividing by the interval boundary, the effect of separating the flaw and the background is shown in Figures 4(a3) and 4(b3), i.e., the flaw detection results of the front and back flaw images by the HHT method.

3.3. **Determination of flaw incident locations.** In this stage, the merged images obtained from flaw detection are used to judge the front and back of the flaw incident position. In this study, the flaw detection results of the front and back flaw images are combined with the OR logic operation to complete the image merging, and the corresponding flaw features are extracted from the front and back images by locating the positions of the flaws in the merged images. Since multiple flaws can occur per image, individual flaws are counted at this stage. We number each flaw and then extract the feature values of the flaw in the original and binarized front and back images (the difference in grayscale means, the difference in grayscale standard deviations, flaw area, and flaw perimeter) and use the random forest method for classification. The detected flaws are individually divided into three categories: front-side flaws, back-side flaws, and non-flaws.

The intensity features and geometric features of the front and back images are extracted for each flaw, respectively, and the corresponding feature values of the front and back of the flaw are subtracted to obtain the difference between the flaws in the two images on the front and back. The brightness of a flaw is the intensity that describes the flaw. The

geometric properties of the flaw reflect the size and shape of the flaw. The front flaws are marked with red circles and the back flaws are marked with blue squares in Figure 5. Taking the front-side flaw as an example, if the front side is focused as shown in Figure 5(a1), the grayscale value of the flaw will be lower and the shape of the flaw will be clearer. If the front-side flaw is in focus on the back side, as shown in Figure 5(b1), the flaw will appear blurry and the intensity value of the flaw will be higher. Flaw shapes with wrong focus after binarization are likely to have broken edges, resulting in flaws that are not closed-form. The area and perimeter of such flaws will be larger. Through these difference analyses, the difference in intensity averages, the difference in intensity standard deviations, and the area and perimeter of the geometric features, the flaws are classified and the positions of the flaws are judged on the front side or the back side.

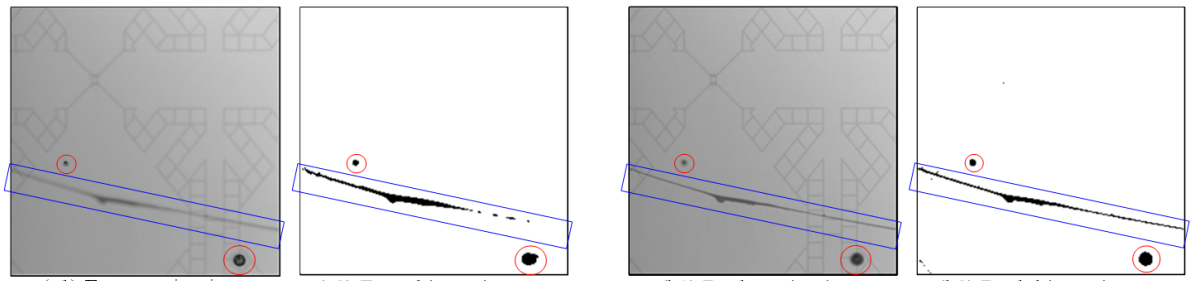

FIGURE 5. Image difference between where the flaws are in focus and where they occur in original and binarized images

The random forest model based on ensemble learning is used to judge the flaw incident location, and each decision tree in the random forest is a different classifier and is used to judge the position of the flaw. Different features can be selected to increase the diversity of the classifier, and the classifier is implemented in parallel processing, so the execution process is quite fast [23]. Decision trees are generated independently to maintain high accuracy and noise immunity when data is imbalanced or missing [10,18]. Through the classification results of the decision trees, the opinions of each tree can be collected to vote on. The category with the highest vote is the incident location of the flaw. Figure 6 is an example of the determination of the flaw incident location using the random forest method. During the flaw detection stage, some background textures and flaws will be detected as potential flaws at the same time. These background textures are misjudged flaws and such misjudged flaws will be classified as a non-flaw type. Therefore, this study classifies each detected flaw into three categories: front-side flaw, back-side flaw, and non-flaw. Figure 7 shows the processed results of three stages including image merging, flaw numbering, and incident location determination in the classification of the detected flaws.

4. **Experiments and Results.** In system development, the Matlab R2013b version is used to implement the proposed algorithms for flaw detection and determination of the location of the flaw incident on the front and back sides of transparent workpieces. The types of equipment used are a personal computer (Intel Core i5 processor, 4 GB*1 RAM, Win7 operating system), a 5-megapixel CCD (Charge Coupled Device), an inspection platform, and a blue coaxial light source. The captured images are resized to 256×256 pixels in a $1:1$ ratio.

In this study, an image is taken as the basic unit of calculation and the detection results are compared with the manually detected images. In terms of fault detection, the recall rate, precision rate, F1 score, and accuracy rate are used as the performance evaluation

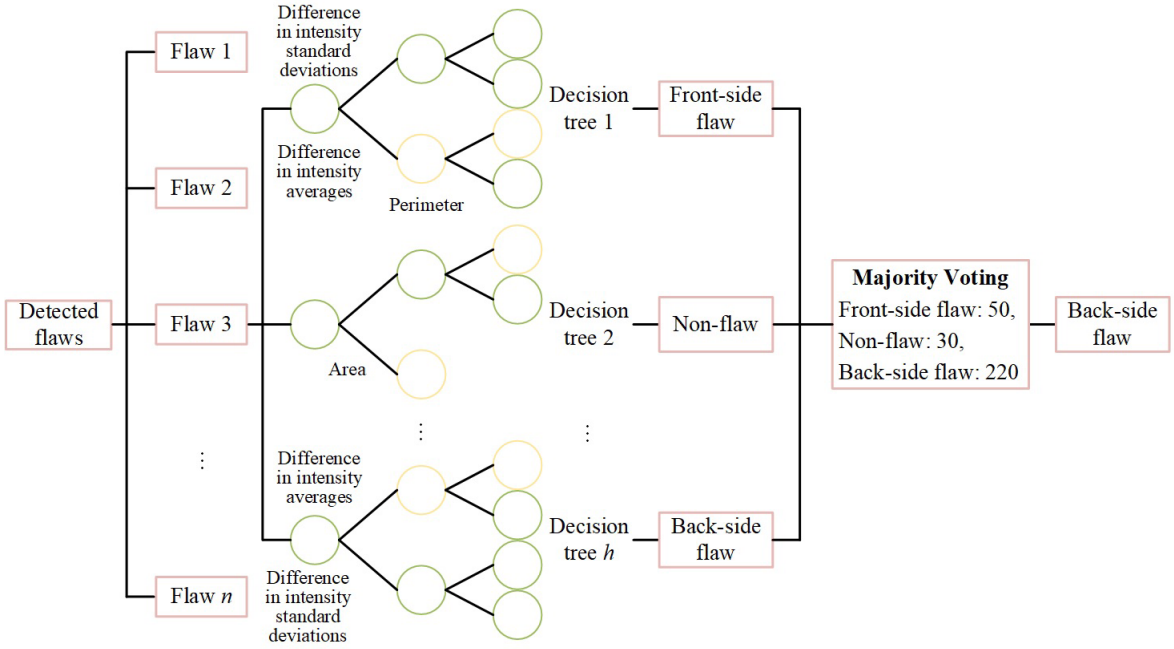

FIGURE 6. An example of the tree structure of the flaw incident location determined by the random forest method

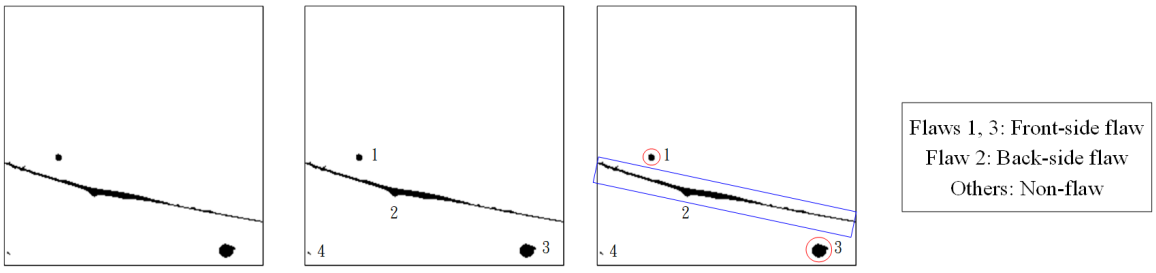

(a) Combined flaw image (b) Numbered flaws in combined image (c) Result image of incident location determination (d) Determination reports

FIGURE 7. The processed results of three stages of the incident location determination in the classification of the detected flaws

indicators of the proposed models. When the above performance indices are higher, the classification performance is better. The recall rate is the number of correctly identified true defects (True Positives, TP) divided by the number of correctly identified true defects (TP) plus the number of true defects incorrectly labeled as non-defects (False Negatives, FN). It can be thought of as the fraction of true defects that are correctly identified in the set of all true defects. The precision rate is the number of correctly identified true defects (TP) divided by the number of correctly identified true defects (TP) plus the number of non-defects incorrectly labeled as defects (False Positives, FP). It can be thought of as the fraction of these detected defects that are true defects. The F1 score is the harmonic mean of precision and recall, taking both metrics into account and giving both metrics equal weight. The accuracy rate is the number of correctly identified true defects (TP) and the number of correctly labeled true non-defects (TN) divided by the total number of testing instances (TP + TN + FP + FN). It represents the rate of correctly identified defects and non-defects over the total number of testing instances. If the dataset is imbalanced (both defect and non-defect classes have significantly different numbers of testing instances), the accuracy rate is not a good metric [32,33].

In terms of determining the flaw incident locations, the accuracy rate is revised as the performance evaluation index with the number of flaws as the basic unit. The detected flaws are judged individually into three types, front-side flaw, back-side flaw, and non-flaw, by the random forest method and they are checked whether each type is classified correctly. The accuracy rate of the number of flaws classified in the correct type to the total number of flaws.

4.1. **Parameter selections of the flaw enhancement procedure.** When a testing image is decomposed by the BEMD scheme, the decomposition process calculates the average envelope through the cubic curve and subtracts the average envelope from the image to obtain a new IMF image. There are many iterations in the process so it takes a lot of time to execute. There are two parameters in BEMD that can be adjusted to improve the execution efficiency, namely the number (i) of IMF frequency images and the threshold value (T) of the stopping criterion SD value.

With the change in the number of decomposed images, each frequency image represents different meanings. When $i = 2$ indicates the information of the testing image divided into two images, the amount of information obtained by the two images is the same and the execution time is short. When the number of decomposed images is larger, it means that there are more iterations and more time is spent. When $i = 5$, the testing image is decomposed into four frequency images and one residual image. The IMF_1 image represents a high-frequency image, which has more image information and obvious texture features. The other IMF frequency images contain less and less information in sequence, and the residual image is a low-frequency image with the remaining information after decomposition. When the image is decomposed into more images, the number of iterations will increase and the time will be longer. Therefore, in this study, $i = 2$ is chosen as the BEMD image decomposition parameter.

The BEMD process ordinarily sets the criterion for stopping the sifting process by calculating the standard deviation (SD). When the stopping criterion SD value is less than the threshold value (T), the first component of the BEMD procedure is generated, which is the first IMF frequency image. A new image is obtained by subtracting the first frequency image from the testing image, and then the new image is used for decomposition to generate other IMF frequency images in sequence. The set of threshold T values will affect the important parameters of the time duration in the iterative process. After setting the T value to 1, the execution time decreased significantly, from 5.11 seconds to 2.6 seconds, but there is no difference in the detection results. Therefore, this study chooses $T = 1$ as the threshold value of the stop standard SD value.

4.2. **Parameter selections of the flaw detection procedure.** After HHT conversion, the flaws have been enhanced and the background has been attenuated. Then, threshold segmentation is required to separate the background and flaws. This study uses interval estimation to calculate the threshold for image binarization. The average value of the grayscale minus s times the standard deviation is set as the standard threshold, and image segmentation was performed to calculate the performance evaluation results. The standard threshold to be set for image segmentation is very important for flaw detection, and the threshold value will affect the result of image segmentation. If the threshold value of the flaw segmentation is set too high, the flaw will have broken edges and the flaw area becomes smaller. Although reducing the threshold value can improve the flaw detection rate, it will also increase the misjudgment of more background textures as flaws, increasing the false alarm rate of normal areas and hurting the subsequent location judgment of flaw occurrence.

After the segmentation threshold experiment with different s times of standard deviation, the performance evaluation result is better if s equals 1.8. When $s = 1.8$, the flaw detection rate is 85.11% in real defects and the false alarm rate is 2.9% in detected defects. Precision-recall (PR) charts help visualize how the choice of threshold affects classifier performance and can even help us choose the best threshold for a particular problem [34,35]. In Figure 8, it can be found that the precision of 1.8 is better and the background misjudgment is small; when $s = 2.2$, the threshold is set too high, although the background is completely removed, and many flaws are also eliminated and the detection effect is not good; when the threshold $s = 1.6$ is set too low, the flaws and background are detected at the same time, resulting in the problem of high misjudgment. The appropriate setting of the threshold value will affect the situation of flaw segmentation and the subsequent determination of the flaw location, so the segmentation of the threshold value selects 1.8 as a parameter, which improves the flaw detection and reduces the misjudgment of the threshold value.

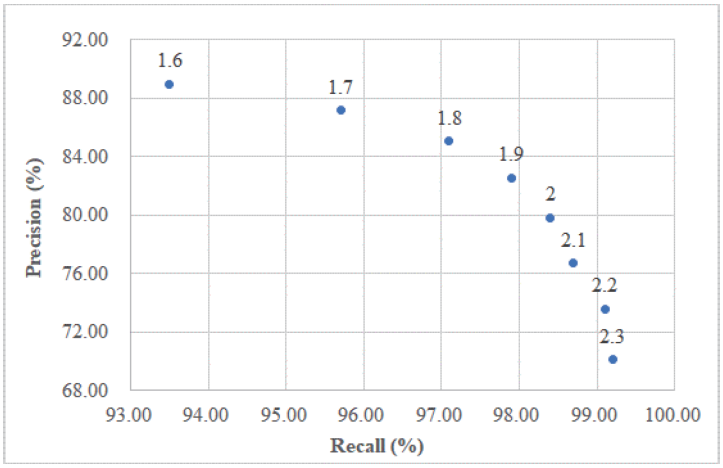

FIGURE 8. A PR chart of different threshold values (s) in performance evaluation of flaw segmentation

4.3. **Parameter selections of the incident location determination procedure.** The random forest method can adjust the structure of the classifier through parameter settings to improve the classification effect. This study will adjust the number and depth of trees to evaluate the classification performance. If the number of trees is set too large, the calculation and classification time will increase, and if the depth of trees is excessively increased, the diversity of the tree will be reduced and the classification effect will also be reduced. The size of the random forest architecture depends on the number of trees (U) to determine how many decision trees are needed in the forest. The number of trees chosen in the random forest method must be large enough to make the error small. The larger the number of forests used and the larger the forest scale, the test error will gradually converge with the increase of the scale, but at the same time, the amount of calculation will also increase, which is prone to overfitting. Usually, 500 decision trees are enough to solve general problems [36]. In this study, the number of trees is used as the parameter for testing, and forests consisting of 150, 200, 250, 300, 350, 400, 450, and 500 decision trees will be tested.

The depth of trees in the random forest method is composed of the different number of features selected for each decision tree to increase the diversity of the forest. The greater the number of selected features in a decision tree, the greater the depth of the decision tree and the greater the effect of a single decision tree, but each decision tree in the forest

is similar, resulting in a decrease in diversity and prediction accuracy. Conversely, it can speed up the processing time and reduce the prediction error. The depth of trees is used as the parameter for testing, and each decision tree can randomly select V features from the 4 features.

According to the combinations of the number of trees and the depth of trees, the two parameters are matched with different setting levels and a total of 32 classifier combinations are tested. The accuracy rate and the execution time of testing are used as indices to evaluate the classification results. The 50 training samples and 30 testing samples are used to adjust the parameters to construct a random forest structure with a better parameter combination and conduct subsequent experiments with large samples. It is found that the more features and decision trees are used, the better the experimental results might not be obtained. When three combinations of ($U = 300$, $V = 1$), ($U = 500$, $V = 2$), and ($U = 500$, $V = 3$) are used to establish the random forests, the diversity of the classifiers can be improved, and the accuracy rate of 95.69% can be achieved. However, using 500 decision trees and more selected features requires a lot of training and testing time, so this study chooses ($U = 300$, $V = 1$) as a suitable parameter setting for the random forest method.

4.4. **Result comparisons of flaw detection and incident location determination by the existing methods and proposed approach.** In large-sample experiments, 462 images are used for large sample experiments in the flaw detection part. In the front and back side determination part of the flaw incident, 208 images are used for training, 150 normal images and 104 flaw images are used for testing, and experiments are carried out with the selected parameter settings. In the flaw detection part, the flaw detection results of the HHT method are summarized as follows, the detection rate of all real defects is 86.67%, the false alarm rate of the detected defects is 2.32%, and the accuracy rate of total testing samples is 99.62%. In the flaw location determination part, after the flaw features are extracted and classified by the random forest model, the accuracy rate is 98.62%.

It will be compared with other methods using performance evaluation indicators to explore the benefits of the proposed approach. The flaw detection is compared with the curvelet transformation (CT) and the flaw location determination is compared with the back-propagation neural (BPN) network. The CT filtering method proposed by Lin et al. [37] used the background removal approach and the multi-angle filtering method was adopted to filter out the background texture and retain the flaws. The curvelet transform is an extension of the wavelet transform and exhibits better directionality and reconstruction [38]. The CT method transfers the image to the frequency domain, decomposes the image to high frequency, and performs filtering processing on the background texture to achieve the effect of background deletion. The testing image is transferred to the frequency domain for 4th-order curvelet transformation, and multi-angle filtering is performed on the characteristics of the background texture ($\pm 30°$, $\pm 40°$, $90°$, $0°$), and the image is inverted to the spatial domain to obtain a background-attenuated image. Then, the filtered image is converted back to the space domain, and the rebuilt image can be easily segmented into the flaw and the background. The process of the CT filtering method achieves the effect of flaw detection as shown in Figure 9.

There are various types of structural textures inside the touch panels. The CT filtering method will perform multi-angle filtering for specific textures. If the testing panel has different background textures, the filtering angles need to be reset. After the filtering angles of the background texture are fixed, it is also necessary to fix the orientation of the workpiece, that is, a fixture is required to fix the orientation of the workpiece to accurately

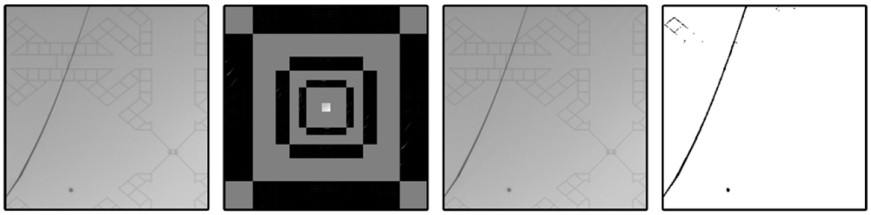

FIGURE 9. The CT filtering method applied to images for flaw detection

attenuate the background texture. In this study, the HHT is used to attenuate the background and enhance flaws, and it can be applied to touch panels with more different types of background textures.

We compare the effects of the CT filtering method and the HHT-based method in flaw detection. The flaw detection rates of all real defects are 85.78% and 86.67%, respectively, and the false alarm rates of the detected defects are 3.75% and 2.32%, respectively, as shown in Table 1. The CT method has a lower detection rate and a higher false alarm rate than the HHT method in flaw detection. This will lead to more misjudgments of flaw locations in subsequent processes. In terms of accuracy rate and F1 score, the HHT method is also superior to the CT method. The HHT method needs to perform the BEMD procedure on the image, and the decomposition process needs to go through many iterations, resulting in a longer execution time of the method, which takes 1.75 seconds. The curvelet conversion has the advantage of fast execution efficiency and takes 0.82 seconds. However, in flaw detection, a fixture is needed to fix the placement of the workpiece, and the CT filtering method of removing the fixed-angle background is only suitable for workpieces with a specific background texture. When processing the flaw detection of workpieces with various background textures, it is necessary to frequently change the parameter settings for the detection. This study proposes applying the HHT method to flaw detection in transparent workpieces. The flaw detection effect is not much different from that of the CT filtering method, but the orientation of the workpiece can be arbitrarily placed without the aid of a fixture in the application, so it can be more widely used in transparent workpieces with different background texture types. Therefore, this study proposes that the HHT method has a good detection effect and a wide range of applications.

In this study, the random forest method is used to judge the front and back positions of flaws, and the same data is used to compare the performance evaluation index with the BPN network. The accuracy rates of the BPN model and the random forest model are

TABLE 1. Performance evaluation results of the curvelet transform method and the proposed approach for flaw detection and incident location determination

Indicators	CT filtering method [37]		Proposed HHT-based method	
Recall (%)	85.78		86.67	
Precision (%)	96.25		97.68	
Accuracy (%)	99.41		99.62	
F1 score (%)	90.71		91.85	
Processing time (sec.)	0.82		1.75	
Side judgment	BPN	Random forest	BPN	Random forest
Accuracy (%)	83.09	95.39	83.62	98.62

83.62% and 98.62%, respectively, as shown in Table 1. Therefore, when using the same feature values with different classifiers, the accuracy rate of the random forest method proposed in this study is better than that of the BPN network model. The classification effect of the random forest method is more sensitive than the BPN network.

4.5. **Flaw detection results from changing different ways of workpiece placement by the existing method and proposed approach.** In automatic inspection, if the workpiece needs to be placed in a fixed position for inspection, it needs to be used together with a jig, which is another equipment expense. The CT method uses a multi-angle filtering method to remove the background texture. It is necessary to fix the position of the workpiece and align the angle and direction of the background texture to accurately attenuate the background. The proposed HHT method uses the BEMD to decompose the image and performs the HT to achieve the effect of flaw enhancement. The workpiece position can be placed arbitrarily and flaws can be detected. When the workpiece is placed in a fixed position with a jig, the angle and direction of the background texture are fixed. Comparing the flaw detection results of the CT method and HHT method, the PR chart shows the influence of CT and HHT on the change of workpiece position as shown in Figure 10. In the case of fixed orientation, the CT method has a better detection effect than any placement method, as shown in Figure 11. When using CT to inspect any placed workpiece, some background textures and flaws will be detected at the same time, as shown in Figure 11. The experimental results show that the HHT method is less restricted in position placement, the workpiece can be placed arbitrarily, and has little impact on the detection effect. From Table 2, there is little difference in the detection effect with or without the fixture, so the impact of HHT conversion on the placement of the sample is small.

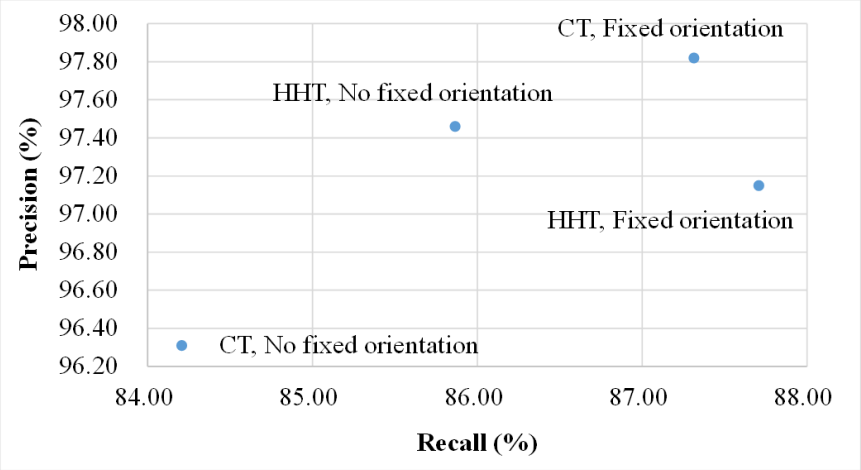

FIGURE 10. A PR chart of flaw detection on panel images with different ways of workpiece placement

5. **Concluding Remarks.** This research incorporates optical flaw detection and side determination of flaw location into the quality control of transparent workpieces. The proposed hybrid approach, combining the Hilbert-Huang transformation and the random forest method, automatically inspects flaws on the workpiece and determines whether the flaws are on the front or back sides. The experimental results show that the method achieves a flaw detection rate of 86.67% in all real defects and a false alarm rate of 2.32% in the detected defects. In the side determination of flaw location, the classification

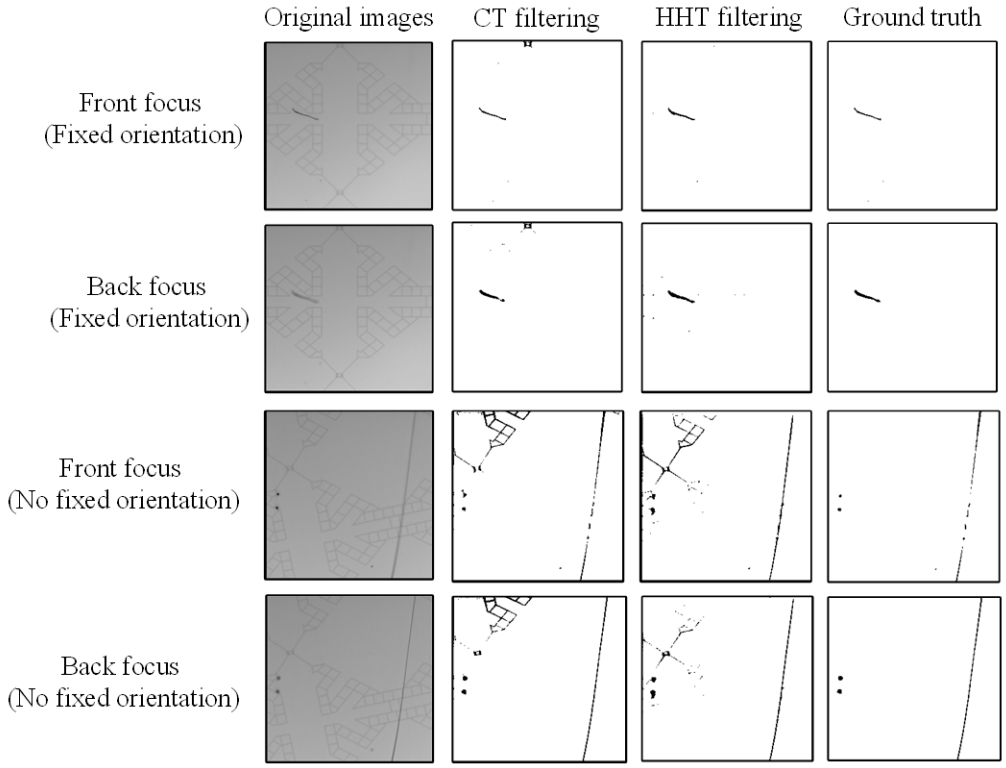

FIGURE 11. Partial results of flaw detection on panel images with different ways of workpiece placement

TABLE 2. Performance evaluation results of flaw detection and classification for different ways of workpiece placement

Methods	Ways of workpiece placement	Precision (%)	Recall (%)	Accuracy (%)
CT method	Fixed orientation	97.82	87.31	99.55
	No fixed orientation	96.31	84.21	99.26
HHT-based method	Fixed orientation	97.15	87.71	99.36
	No fixed orientation	97.46	85.87	99.41

accuracy reached 98.62%. This HHT-based method can arbitrarily place the workpiece without using a fixture to orient the test object, so it can be used to inspect transparent workpieces with a variety of background textures. Therefore, this proposed approach not only achieves a good detection rate but also has a wide range of applications. However, there are still some issues that need refinement, and the proposed approach would benefit greatly from further studies in the following three directions: 1) improvement in execution efficiency of the HHT method; 2) determination of flaw locations when the front and back flaws partially overlap; 3) integration of the proposed approach into production systems in a real-time industrial environment.

Acknowledgment. This research received financial support through the Grant MOST 109-2221-E-324-014 provided by the Ministry of Science and Technology, Taiwan.

REFERENCES

[1] J. Xu, N. Xi, C. Zhang, Q. Shi and J. Gregory, A geometry and optical property inspection system for automotive glass based on fringe patterns, *Optica Applicata*, vol.40, no.4, pp.827-841, 2010.

[2] H.-D. Lin, Y.-C. Lo and C.-H. Lin, Computer-aided transmitted deformation inspection system for see-through glass products, *International Journal of Innovative Computing, Information and Control*, vol.18, no.4, pp.1217-1234, 2022.
[3] W. Ming, F. Shen, X. Li, Z. Zhang, J. Du, Z. Chen and Y. Cao, A comprehensive review of defect detection in 3C glass components, *Measurement*, vol.158, 107722, 2020.
[4] L. Lettry, M. Perdoch, K. Vanhoey and L. Van Gool, Repeated pattern detection using CNN activations, *2017 IEEE Winter Conference on Applications of Computer Vision (WACV)*, pp.47-55, 2017.
[5] T. Hiraoka, Generation of fingerprint-pattern images using cosine-wave-weight smoothing filter, *ICIC Express Letters*, vol.16, no.2, pp.153-158, 2022.
[6] H.-D. Lin and H.-H. Tsai, Automated industrial inspection of touch panels using computer vision, *Proc. of the 2013 International Conference on Image Processing, Computer Vision, and Pattern Recognition (IPCV)*, vol.1, pp.351-357, 2013.
[7] M.-H. Hung and C.-H. Hsieh, A novel algorithm for flaw inspection of touch panels, *Image and Vision Computing*, vol.41, no.21, pp.11-25, 2015.
[8] L. Q. Liang, D. Li, X. Fu and W. J. Zhang, Touch screen flaw inspection based on sparse representation in low-resolution images, *Multimed. Tools Appl.*, vol.75, no.5, pp.2655-2666, 2016.
[9] Y.-S. P. Chiu and H.-D. Lin, Creation of image models for inspecting visual flaws on capacitive touch screens, *Journal of Applied Engineering Science*, vol.16, no.3, pp.333-342, 2018.
[10] C. X. Jian, J. Gao and Y. Ao, Automatic surface flaw detection for mobile phone screen glass based on machine vision, *Applied Soft Computing*, vol.52, pp.348-358, 2018.
[11] R. Ye, C. S. Pan, M. Chang and Q. Yu, Intelligent flaw classification system based on deep learning, *Advances in Mechanical Engineering*, vol.10, no.3, pp.1-7, 2018.
[12] J. Lei, X. Gao, Z. Feng, H. Qiu and M. Song, Scale insensitive and focus driven mobile screen flaw detection in industry, *Neurocomputing*, vol.294, pp.72-81, 2018.
[13] R. Ye, M. Chang, C. S. Pan, C. A. Chiang and J. L. Gabayno, High-resolution optical inspection system for fast detection and classification of surface flaws, *International Journal of Optomechatronics*, vol.21, no.1, pp.1-10, 2018.
[14] A. Carlson and T. Le, Correlation of wafer backside flaws to photolithography hot spots using advanced macro inspection, *Proceedings of SPIE*, vol.6152, pp.1123-1129, 2006.
[15] H. Minami, F. Matsumoto and S. Suzuki, Prospects of LCD panel fabrication and inspection equipment amid growing demand for increased size, *Hitachi Review*, vol.56, no.3, pp.63-69, 2007.
[16] M. D. Gevigney, Novel surface scanning inspection system for opaque and transparent substrates using laser Doppler velocimetry, *2018 29th Annual SEMI Advanced Semiconductor Manufacturing Conference (ASMC)*, pp.23-28, 2018.
[17] Y.-M. Kim, I.-U. Yoon, H. Myung and J.-H. Kim, Bi-directional convolutional recurrent reconstructive network for welding defect detection, *IEEE Access*, vol.9, pp.135316-135325, 2021.
[18] N. E. Huang, Z. Shen, S. R. Long, M. C. Wu, H. H. Shih, Q. Zheng, N.-C. Yen, C. C. Tung and H. H. Liu, The empirical mode decomposition and the Hilbert spectrum for nonlinear and non-stationary time series analysis, *Proceedings of the Royal Society of London. Series A: Mathematical, Physical and Engineering Sciences*, vol.454, no.1971, pp.903-995, 1998.
[19] S. R. Long, Applications of HHT in image analysis, in *Hilbert-Huang Transform and Its Applications*, World Scientific, 2014.
[20] M. F. Guo, N. C. Yang and W. F. Chen, Deep-learning-based fault classification using Hilbert-Huang transform and convolutional neural network in power distribution systems, *IEEE Sensors Journal*, vol.19, no.16, pp.6905-6913, 2019.
[21] Y. Lu and R. Lu, Fast bi-dimensional empirical mode decomposition as an image enhancement technique for fruit flaw detection, *Computers and Electronics in Agriculture*, vol.152, pp.314-323, 2018.
[22] Y. Qin, L. H. Qiao, Q. R. Wang, Z. Xiao and C. H. Zhu, Bidimensional empirical mode decomposition method for image processing in sensing system, *Computers & Electrical Engineering*, vol.68, pp.215-224, 2018.
[23] M. E. Abdulmunem and A. A. Badr, Hilbert transform and its applications: A survey, *International Journal of Scientific & Engineering Research*, vol.8, no.2, pp.699-704, 2017.
[24] B.-K. Kwon, J.-S. Won and D.-J. Kang, Fast defect detection for various types of surfaces using random forest with VOV features, *International Journal of Precision Engineering and Manufacturing*, vol.16, no.5, pp.965-970, 2015.

[25] M. Belgiu and L. Dragut, Random forest in remote sensing: A review of applications and future directions, *ISPRS Journal of Photogrammetry and Remote Sensing*, vol.114, pp.24-31, 2016.
[26] S. Kamalalochana and G. Nirmala, Optimizing random forest to detect disease in apple leaf, *International Journal of Engineering and Advanced Technology*, vol.8, no.5, pp.224-229, 2019.
[27] N. J. Shipway, T. J. Barden, P. Huthwaite and M. J. S. Lowe, Automated flaw detection for fluorescent penetrant inspection using random forest, *NDT & E International*, vol.101, pp.113-123, 2019.
[28] X. Dong, C. J. Taylor and T. F. Cootes, A random forest-based automatic inspection system for aerospace welds in X-ray images, *IEEE Transactions on Automation Science and Engineering*, vol.18, no.4, pp.2128-2141, 2021.
[29] E. Jr Piedad, J. I. Larada, G. J. Pojas and L. V. V. Ferrer, Postharvest classification of banana (Musa acuminata) using tier-based machine learning, *Postharvest Biology and Technology*, vol.145, pp.93-100, 2018.
[30] A. Verikas, A. Gelzinis and M. Bacauskiene, Mining data with random forests: A survey and results of new tests, *Pattern Recognition*, vol.44, no.2, pp.330-349, 2011.
[31] V. Y. Kulkarni and P. K. Sinha, Random forest classifiers: A survey and future research directions, *International Journal of Advanced Computing*, vol.36, no.1, pp.1144-1153, 2013.
[32] D. M. W. Powers, Evaluation: From precision, recall and F-measure to ROC, informedness, markedness & correlation, *Journal of Machine Learning Technologies*, vol.2, no.1, pp.37-63, 2011.
[33] H. R. Sofaer, J. A. Hoeting and C. S. Jarnevich, The area under the precision-recall curve as a performance metric for rare binary events, *Methods in Ecology and Evolution*, vol.10, pp.565-577, 2019.
[34] K. H. Brodersen, C. S. Ong, K. E. Stephan and J. M. Buhmann, The binormal assumption on precision-recall curves, *2010 20th International Conference on Pattern Recognition*, pp.4263-4266, 2010.
[35] J. Cook and V. Ramadas, When to consult precision-recall curves, *The Stata Journal*, vol.20, no.1, pp.131-148, 2020.
[36] F. B. Santana, W. B. NetoRonei and J. Poppi, Random forest as one-class classifier and infrared spectroscopy for food adulteration detection, *Food Chemistry*, vol.293, no.30, pp.323-333, 2019.
[37] H.-D. Lin, C.-Y. Lin and C.-H. Lin, Detection of fishbones in fish floss products using curvelet transform based square-ring band-highpass filtering techniques, *International Journal of Innovative Computing, Information and Control*, vol.17, no.1, pp.31-47, 2021.
[38] P. Anandan and R. S. Sabeenian, Fabric defect detection using discrete curvelet transform, *Procedia Computer Science*, vol.133, pp.1056-1065, 2018.

Author Biography

Hong-Dar Lin is currently a professor in the Department of Industrial Engineering and Management at Chaoyang University of Technology, Taiwan. He received his Ph.D. degree in industrial engineering from the University of Missouri-Columbia, USA in 1994. His research interests are in quality management, applications of machine vision systems, automated inspection and metrology, machine learning, pattern recognition, and algorithms of information fusion.

Zi-Ting Qiu received the B.Sc. and M.Sc. degrees in industrial engineering and management from Chaoyang University of Technology, Taiwan, in 2018 and 2020, respectively. Her research interests include quality management, applications of machine vision systems, automated inspection and metrology, and pattern recognition.

Chou-Hsien Lin is currently pursuing the M.Sc. degree in Civil Engineering at The University of Texas at Austin, USA. He received the B.Sc. degree in architectural engineering from the same institution in 2020. His research interests include indoor air quality, exposure pathways of air pollutants, and the health effects of volatile organic compounds in the built environment.